Journal of the Taiwan Institute of Chemical Engineers 129 (2021) 40–51

Contents lists available at ScienceDirect

Journal of the Taiwan Institute of Chemical Engineers

journal homepage: www.elsevier.com/locate/jtice

Lipid-assisted synthesis of magnesium-loaded hydroxyapatite as a potential bone healing material

Yu-Hsin Chen[a,1], Yu-Sheng Yu[a,1], Pao-Tao Yu[a], Hsu-Wei Fang[b], Ying-Chih Chang[c,d,*], Kevin C.W. Wu[a,e,**]

[a] Department of Chemical Engineering, National Taiwan University, No. 1, Sec. 4, Roosevelt Road, Taipei 10617, Taiwan
[b] Department of Chemical Engineering and Biotechnology, National Taipei University of Technology, 1, Sec. 3, Zhongxiao E. Rd., Taipei 10608, Taiwan
[c] Genomics Research Center, Academia Sinica, Taipei, Taiwan
[d] Department of Chemical Engineering, Stanford University, Stanford, CA, USA
[e] Institute of Biomedical Engineering and Nanomedicine, National Health Research Institutes, 35, Keyan Road, Zhunan Town, Miaoli County 350, Taiwan

ARTICLE INFO

Article History:
Received 15 June 2021
Revised 11 September 2021
Accepted 12 September 2021
Available online 28 September 2021

Keywords:
Hydroxyapatite
Magnesium
Phosphatidylcholine
Bone healing
MG-63 osteoblast-like cells

ABSTRACT

Background: Magnesium-loaded hydroxyapatite (Mg@HAp) is a potential biomaterial for bone healing application but has not been comprehensively synthesized yet.
Methods: In this study, we utilize phosphatidylcholine (PC)-assisted method for synthesizing Mg@HAp with controllable Mg amount from 1.44 to 10.64 wt%. It is proposed that the negatively charged phosphate functional group of PC could act on cations (i.e. Mg^{2+} or Ca^{2+}), which provides stable nucleation for the formation of Mg@HAp.
Significant findings: By optimizing the synthesis conditions, we successfully prepared a Mg@HAp with a relatively low crystallinity which is similar to human bone structure, as evidenced by XRD measurement. The *in vitro* test of bone cells (MG-63) shows that the release of Mg^{2+} ions from Mg@HAp enhances cellular proliferation and differentiation. We believe the synthesized Mg@HAp would be a promising biomaterial in orthopedic applications.

1. Introduction

Bone regeneration is a bodily process that occurs after injuries, such as bone fractures, happen. Eventually, it will make the injured part indistinguishable from the uninjured part. However, in some severe cases, including non-union fractures and defects caused by tumor resection surgery, the bone can no longer recover through the regeneration process [1,2].

In cases which bone defects are not self-regenerative, methods involving autologous or allogeneic bone grafts and synthetic bone substitute materials shall apply [3]. Among these treatments, the synthetic bone substitute is getting more and more popular because it does not include the donor-site morbidity of autologous bone grafts and the risk of rejection of allogeneic bone grafts. Furthermore, synthetic bone substitutes can be classified into non-biodegradable materials and biodegradable materials. A well-known example of non-biodegradable materials is poly (methyl methacrylate) (PMMA), also known as bone cement [4,5]. Biodegradable materials, for instance, inorganic ceramics, e.g. Calcium Phosphate (CaP), is one of the most popular research topics [6,7]. Although CaP does not possess osteoinduction capacity, they certainly have bone conduction capacity and significant ability to directly bind to the bone [8]. To make CaP a better bone repairing material, studies have utilized organic and inorganic substances to modify the properties of CaP [9,10]. On the other hand, how these modifications affect the phase transition of CaP is also attracting interest [11].

Currently, the most commonly used CaP in clinics are hydroxyapatite (HAp) and biphasic cement, which are usually mixtures of HAp and β-tricalcium phosphate (β-TCP) [12,13]. Among those, HAp is thermodynamically the most stable crystalline phase. Combinations of tough polymer and HAp have been applied to mimic the organic-inorganic composition of natural bone. The most significant organic component in the bone structure is collagen, which promotes the production of nanosized crystals of CaP aligned in the cortical bone [14]. Nonetheless, how the highly ordered structure is formed from the combination of organic and inorganic molecules is still unclear [15–17]. Additionally, the inorganic component of the natural bone is nonstoichiometric apatite which is low crystalline and contains

Abbreviation: HAp, hydroxyapatite; PC, phosphatidylcholine

* Corresponding author at: Genomics Research Center, Academia Sinica, Taipei, Taiwan.
** Corresponding author at: Department of Chemical Engineering, National Taiwan University, No. 1, Sec. 4, Roosevelt Road, Taipei 10617, Taiwan.
E-mail addresses: hwfang@ntut.edu.tw (H.-W. Fang), yingchih@gate.sinica.edu.tw (Y.-C. Chang), kevinwu@ntu.edu.tw (K.C.W. Wu).

[1] These authors contributed equally to this work.

https://doi.org/10.1016/j.jtice.2021.09.019
1876-1070/

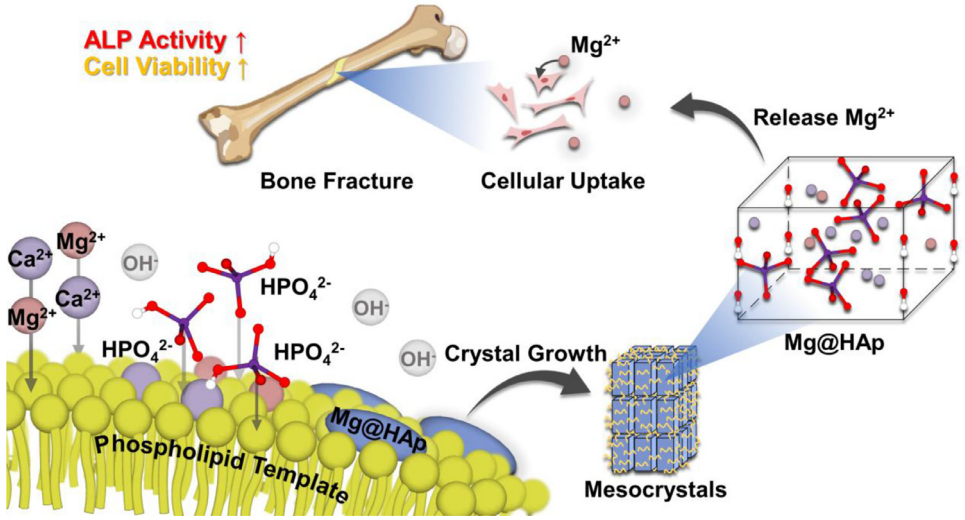

Scheme 1. Illustration of the lipid-assisted synthesis of Mg@HAp and its bone healing application. Where the phospholipid acts as a template for the Mg@HAp. The resulting structure of Mg@HAp from this process will be bone-liked mesocrystals. The incorporated Mg ions in Mg@HAp can be released and further uptake by the bone cells.

cationic and anionic substitution [18]. Properties of synthetic HAp such as degradation rate, bioactivity, and mechanical strength can be controlled through anionic or cationic substitutions as well [19,20].

Magnesium (Mg), the most abundant cationic substitution in natural bone, is crucial for bone health [21,22]. Approximately 50–60% of Mg is stored in the bone matrix of the human body, acting as surface substituents of the HAp mineral component of bone [23]. Moreover, Mg ions can increase the adhesion, growth, and alkaline phosphatase (ALP) activity of osteoblasts and bone mesenchymal stem cells (BMSCs), resulting in promoting the differentiation and enhancing bone formation and integration with host bone [24,25]. The synthetic method of incorporating magnesium ions into HAp lattice has been widely studied. Nonetheless, the maximum amount of Mg incorporated in synthetic HAp has been limited since Mg acts as an inhibitor in the crystallization process of calcium phosphate and destabilizes the structure of HAp [26–28]. Beside, the high hydration energy of Mg makes the preparation of high Mg-content minerals difficult in aqueous solution and at physiological temperature [29], unless paired anionic substitutions such as carbonate or fluoride are simultaneously incorporated with Magnesium ions. Ren et al. synthesized Mg-doped HAp by the wet-chemical precipitation method at 90 °C with the percentage of Mg substitution (Mg / (Mg + Ca)) in HAp between 5 and 7 mol% [30]. Liangzhi et al. managed to synthesize Mg-substituted HAp whiskers by hydrothermal method with acetamide as a homogeneous precipitation reagent [24]. The molar ratio of Mg / (Mg + Ca) could be facilely changed from 1.61 to 6.14 mol%. Cacciotti et al. reported Mg substituted HAp nanopowders, whose Mg content ranged between 0.6 and 2.4 wt% [31]. Landi et al. used the wet-chemical method to synthesize Mg-doped HAp with up to 3.2 wt% of Mg [21]. According to these researches, there are some effects for HAp properties by increasing the content of Mg in HAp: (i) the crystallinity decreasing, (ii) the incorporation of HPO_4^{2-} increasing, and (iii) the extent of dissolution increasing [32,33].

The preparation method of HAp can be divided into the wet method, the dry method, the high-temperature method, and the combination of these methods. The wet method is the most universal one because it provides accurate control of morphology and the size of the particles in small batch production. By modifying the wet synthesis method, we can mimic biomineralization to create a structure that is similar to bioapatite. Feng et al. used liposomes to synthesize HAp [34,35]. They concluded that the vesicle membrane of phospholipids plays an essential role in the mineralization of calcium phosphate. These lipid-assisted synthesized HAp have a chemical composition similar to natural HAp. Huang et al. also observed that lipid-bonded HAp has higher biocompatibility and is beneficial to therapy of bone disease and applications [36]. Although the synthesis of HAp by using liposome as a model has been investigated, there is no study on the substitution of Mg ions in the lattice of HAp in a lipid-assisted system.

Phosphatidylcholine(PC) is one of the phospholipids which composes most of the biological membrane [37]. It consists of a zwitterionic head, a phosphate group, and two non-polar fatty acid chain tails [38]. Phosphatidylcholine can be classified into zwitterionic surfactant, which would have the negatively charged lipid phosphate functional group to interact with Ca and Mg ions [39–41]. Yu et al. prepared mesocrystals of high-magnesian calcite in lipid solution [42]. Therefore, it is conceivable that the surface of the lipid membrane is involved in the nucleation of Mg-loaded HAp (Mg@HAp) particles.

In this work, we aim to synthesize Mg@HAp powders with controllable Mg contents which possess bioactivity, biocompatibility, osteoconductivity, and bioresorbability as potential bone healing material (Scheme 1)

2. Materials and methods

2.1. Materials

Calcium chloride (≥97%), Magnesium chloride (≥98%), Ammonium phosphate dibasic (≥98%), L-α-Phosphatidylcholine from soybean, Type IV-S, Enzymatic (≥30%), Sodium hydroxide (≥97.0%), Potassium bromide (≥99.0%), Dimethyl sulfoxide (≥99.7%), Thiazolyl Blue Tetrazolium Bromide (98%), Triton™ X-100, 2-Amino-2-methyl-1-propanol (≥99.0%), 4-Nitrophenyl phosphate disodium salt hexahydrate (pNPP), Tris-Buffer and 4-Nitrophenol (p-NP) were purchased from Sigma Aldrich. Magnesium chloride hexahydrate (99%) was purchased from J.T. Baker. Ethyl Acetate (≥99.5%), Hydrochloric acid (37%), and Nitric acid (≥69%) were purchased from Honeywell. Dulbecco's Phosphate Buffered Saline (10X), Penicillin-Streptomycin-Amphotericin B Solution, and Trypsin-EDTA (10X) were purchased from Biological Industry. Minimum Essential Medium alpha (MEM-α), Fetal bovine serum (FBS), and Trypan blue stain were purchased from Gibco.

All chemicals were used directly after being received without further purification.

2.2. Synthesis of Mg@HAp

Ammonium phosphate dibasic (0.12 M) was added to a 250 mL serum bottle and dissolved by 125 mL of deionized (DI) water while stirred by a magnetic stirrer. Calcium chloride (x M) and magnesium chloride (y M) were added to another 250 mL round-bottom flask and dissolved by 125 mL of deionized water while stirred by a magnetic stirrer. The total concentration of calcium chloride and magnesium chloride is 0.12 M ($x + y = 0.12$). The pH values of the two solutions were adjusted to 9.00 by 1 M NaOH or 1 M HCl, respectively. Then, magnesium/calcium solution was dropwise added into ammonium phosphate dibasic solution about 2 mL per minute. The mixture was stirred for 15 min before aged in a 37 °C water bath. After 5 to 19 h of aging, the precipitate was collected by centrifugation at 20,000 g for 5 min. The resulting solid was washed with deionized water 5 times. The purified solid was dried by the lyophilizer for at least 24 h. The sample label and the parameters of Ca/Mg concentration were shown in Table 1. The scheme of the typical process was shown in the supporting information S3.

2.3. Synthesis of Mg@HAp-PC

A lipid thin film was prepared by dissolving 4.5 mmol of L-α-phosphatidylcholine (PC) in 30 mL of ethyl acetate (EA) followed by 15 min of sonication. The mixture was placed in a 500 mL round bottom flask and followed by rotary evaporation at 100 rpm, 40 °C for 10 min. The solution of 125 mL of calcium chloride (x M) and magnesium chloride (y M) at pH 9.00 was mixed with the PC film. The total concentration of calcium and magnesium ions is 0.12 M ($x+ y=$ 0.12). After the solution mixture was sonicated for 20 min and adjusted to pH 9.00 again, 125 mL of ammonium phosphate dibasic solution (0.12 M, pH 9.00) was dropwise added into it with 2 mL/min and stirred for 15 min. The solution was incubated under quiescence and physiological temperature at 37 °C for 5 to 19 h in water bath. After aging, the final pH value was in the range of 7.0–7.6. After an addition of 10 mL of EA to the solution mixture, the calcium phosphate precipitate was collected by centrifugation (20,000 g for 5 min). Additional 10 mL deionized water and 10 mL EA were added to wash the solid for 5 times. The sample label and the parameters of Ca/Mg concentration were shown in Table 2. The scheme of the typical process was shown in the supporting information S4.

Table 1
The sample label and the synthesis parameters for Mg@HAp.

Sample	Concentration of Ca^{2+} (M)	Concentration of Mg^{2+} (M)
HAp	0.12	0
Mg@HAp (Ca/Mg = 10)	0.109	0.0109
Mg@HAp (Ca/Mg = 5)	0.1	0.02
Mg@HAp (Ca/Mg = 1)	0.06	0.06

Table 2
The sample label and the synthesis parameters for Mg@HAp-PC.

Sample	Concentration of Ca^{2+} (M)	Concentration of Mg^{2+} (M)	Amount of Phosphatidylcholine (mmol)
HAp-PC	0.12	0	4.5
Mg@HAp-PC (Ca/Mg = 10)	0.109	0.0109	4.5
Mg@HAp-PC (Ca/Mg = 5)	0.1	0.02	4.5
Mg@HAp-PC (Ca/Mg = 1)	0.06	0.06	4.5
Mg@HAp-1.5PC (Ca/Mg = 5)	0.1	0.02	6.75

2.4. Characterization of the materials

Powder X-ray diffraction (PXRD) was performed on Rigaku MiniFlex or Rigaku Ultima IV with Cu Kα radiation (λ = 1.5418 Å) to identify the crystal structure of Mg@HAp.

The field emission scanning electron microscope images were taken with Hitachi S-4800. All the samples were taped on the carbon conductive tape then kept under vacuum to remove the moisture content, followed by sputtering of Pt coating.

Element analysis was conducted with Agilent 7700e ICP-MS. All the samples were digested in aqua regia (0.5 mg/mL) and further diluted to 1000 ppb by 2 wt% nitric acid. The digested samples were filtered by 0.22 μm nylon syringe filters before being injected into the instrument. The calibration curves were built by preparing magnesium, calcium, and phosphorus standard solution of 0, 62.5, 125, 250, 500, and 1000 ppb.

The high-resolution transmission electron microscope images were taken with JEOL JEM-2010. Each powder sample was suspended in ethanol (0.02 mg/mL) and sonicated for 30 min. 10 μL of the suspensions were dropped onto the copper grids and dried at 80 °C. The copper grids were then freeze-dried for at least 24 h.

Fourier-transform infrared (FTIR) spectra were measured with Perkin Elmer Spectrum 100 at a resolution of 4 cm^{-1}. The spectra were detected over the range of 4000–450 cm^{-1}. Samples for FTIR measurement were prepared by mixing vacuum-dried powders with potassium bromide (KBr) by an appropriate ratio (KBr / sample < 1 / 100, w / w) and pressing into translucent discs.

X-ray photoelectron spectroscopy (XPS) was performed with Thermo Scientific Theta Probe Angle-Resolved XPS System to identify the oxidation states of magnesium and oxygen. Before measurement, the spectra were calibrated with reference to C1s at a binding energy of 284.5 eV.

Zeta potentials of samples were measured with Malvern Zetasizer Nano. Samples were dispersed in deionized water (0.1 mg / mL) and sonicated for 1 h before being measured. The pH value of all suspensions was neutral (7.00 ± 0.80) All the measurements were repeated 3 times at 25 °C

The degradation rates of the samples were tested. 50 mg (W_i) of samples were soaked in 10 mL of PBS for 1, 2, 3, and 4 weeks respectively. The temperature was controlled at 37 °C by a thermostatic water bath. At the predetermined time, the mixtures were centrifuged at 4000 g for 10 min to remove the supernatants. Next, precipitated pellets were washed with 10 mL of deionized water and freeze-dried for 24 h. The dry samples were weighed (W_f) to calculated the degradation rates using the following equation:

$$\text{Degradation \%} = (W_i - W_f) / W_i \times 100.$$

The degradation rate was recorded as mean ± standard deviation for $n = 3$.

2.5. Cell culture

Human osteoblast-like cell line MG-63 was used to evaluate the biocompatibility and proliferation-promoting properties of Mg@HAp particles. MG-63 was cultured in T75 flasks with 10 mL Minimum Essential Medium α (MEM-α) containing 10% Fetal bovine serum (FBS) and 1 % Pen-Strep-Ampho.B (P/S/A). The cells were incubated at 37 °C under 5 % of CO_2 in air and subcultured every 3 to 5 days.

2.6. MTT assay

MTT assay was performed to determine the viability and proliferation of MG-63 cells. The mitochondria are the most sensitive organelles in the cell to environmental factors, so their physiological status can represent the whole cell's physiological state. The mitochondrial succinate dehydrogenases of living cells convert the yellow water-soluble MTT (3-(4,5-dimethylthiazol-2-yl)-2,5-diphenyltetrazolium

bromide) dye into purple insoluble formazan [43]. After dissolving the formazan in DMSO, the absorbance at 570 nm can be used to determine the activity of the mitochondria, the viability of cells. So, this method can be used to evaluate the compatibility of biomaterials for cell lines. The following is the typical procedure of MTT Assay and the preparation of the reagents is provided in supporting information S.1.

(1) 100 μL of MG-63 cell suspension (1×10^5 cells/mL) was transferred into each well of a 96-well cell culture plate. The cells were incubated at 37 °C for 24 h in a humidified atmosphere containing 5 % CO_2.
(2) Culture medium was replaced with 100 μL of materials for the concentration: 0 mg/mL (control group), 0.1 mg/mL, 1 mg/mL.
(3) Incubated cells for 1, 3, 5, 7, and 14 days, separately.
(4) The culture medium was aspirated from the plates and the cells were washed with PBS twice. 100 μL of the MTT solution was added to each well and the plate was further incubated for 3 h at 37 °C.
(5) MTT solution was replaced with 100 μL of DMSO. The plate was incubated at room temperature for 10 min and subsequently subjected to an ELISA reader equipped with a 570 nm filter for colorimetric measurement.
(6) Each experimental group was done for three repetitions (n = 3).

2.7. ALP assay

Alkaline phosphatase (ALP) is an enzyme of osteoblasts, and its expression activity is a distinct feature of osteoblast differentiation. ALP is considered to be an important indicator for the mineralization of bone and is a phenotypic marker for osteoblasts. Under alkaline conditions, ALP reacts with 4-nitrophenyl phosphate (p-NPP) and forming yellow p-nitrophenol (p-NP) [44]. The absorbance at 405 nm can be used to determine the concentration of p-NP. The preparation of the reagents is provided in supporting information S.2.The standard procedures of ALP assay are as follow:

(1) 100 μL of MG-63 cell suspension (1×10^5 cells/mL) was transferred into each well of a 96-well cell culture plate. The cells were incubated at 37 °C for 24 h in a humidified atmosphere containing 5 % CO_2.
(2) Culture medium was replaced with 100 μL of materials for the concentration: 0 mg/mL (control group) and 1 mg/mL.
(3) Incubated cells for 3, 5, 7, and 14 days, separately.
(4) The culture medium was aspirated from the plates and the cells were washed with PBS twice.
(5) 100 μL of the 0.1 % Triton X-100 solution was added to each well and the plate was further incubated for 1 h at 37 °C.
(6) In a dark environment, took 50 μL of cell extract and p-NP solution (0, 6.25, 12.5, 25, 50, 100 μM) to 96-well plate and added 200 μL substrate buffer to each well for 1 h incubation at 37 °C.
(7) The reaction was terminated by adding 100 μL of 1 N NaOH.
(8) Used ELISA reader to acquire the absorbance at 405 nm.
(9) The calibration curves were built by the absorbance of p-NP standard solution of 0, 6.25, 12.5, 25, 50, and 100 μM, respectively. The ALP contents of sample were attained by substituting the absorbance into the calibration curve.
(10) Each experimental group was done for three repetitions (n = 3).

2.8. Cellular uptake

The amount of Mg uptake by the MG-63 cell line has been analyzed in this study. 1×10^4 of MG-63 cells were cultured in the well of 96-well plate with 100 μL of MEM-α containing 1 mg/mL of samples. The cells were incubated for 3 days, and the medium was collected to measure the Mg concentration by ICP-MS. It was calculated the Mg ions of cell uptake by using the blank test and original solution concentration.

2.9. Statistical analysis

Data represent the mean ± standard deviation for three replicates. Statistical analysis was carried out on cellular tests using the one-way analysis of variance (ANOVA). * represent the statistically significantly difference between sample and control ($^*p < 0.05$, $^{**}p < 0.01$, $^{***}p < 0.001$).

3. Results and discussion

3.1. Characterizations of Mg@HAp-PC

To understand the influence of phosphatidylcholine on the formation of Mg@HAp crystal, we first synthesize Mg@HAp and Mg@HAp-PC with the ratio Ca: Mg = 1: 0 and simply call these sample HAp and HAp-PC. The aging time of these two samples was 19 h. The FTIR spectra and the XRD patterns of HAp and HAp-PC are shown in Fig. 1. In Fig. 1 (a), the IR peaks at 602 and 561 cm^{-1} are assigned to $\nu 4$ vibration of the PO_4^{3-} antisymmetric bending (O-P-O mode), which can be found in the typical spectra of HAp [45,46]. The peak at 962 cm^{-1} is attributed to $\nu 1$ (symmetric stretching mode) of PO_4^{3-}, and the peaks at 1027 and 1105 cm^{-1} are assigned to $\nu 3$ (asymmetric stretching vibrational mode) of PO_4^{3-} [47–49]. The peaks at 1640 and 1650 cm^{-1} result from vibrations of CO_3^{2-} [49,50]. Comparing the spectra of HAp and HAp-PC, we can find that there are carbonyl band at 1740 cm^{-1}, the antisymmetric vibrations of PO_2 at 1233 cm^{-1}, and the $\delta(CH_2)$ scissoring vibrations at 1466 cm^{-1} in the spectrum of HAp-PC [51]. Also, the signals observed between 2800 and 3100 cm^{-1} correspondings to the symmetric and asymmetric stretching vibrations from the CH_2 and CH_3 groups [52]. The XRD patterns of HAp and HAp-PC were shown in Fig. 1 (b). It indicates that HAp synthesized in the PC system has a lower crystallinity than that without PC. The inverted triangle in Fig. 1 (b) indicates the characteristic peaks of HAp.

To further monitor the transformation of the Mg@HAp crystal phase over time under the influence of magnesium ions and different PC concentrations, the condition of Ca/Mg ratio = 5 was chosen, and their XRD patterns are shown in Fig. 2. All the results indicated that the presence of PC would make the crystallinity of Mg@HAp lower. Fig. 2 (a) shows that the crystallinity of Mg@HAp reached a maximum after 5 h of aging. Fig. 2 (b) indicated that the HAp-PC is still amorphous after 5 h of aging, and, eventually shows the characteristic peak of HAp. Nonetheless, Fig. 2 (c) shows that if the amount of PC increases to 1.5 times, the crystalline phase will not occur after 11 h of aging. We finally choose Mg@HAp-PC for further analysis.

High-resolution TEM was performed to observe the crystal orientation differences in Mg@HAp (Ca/Mg = 5) and Mg@HAp-PC (Ca/Mg = 5).

In Fig. 3 (a-1) and (b-1), the selected area electron diffraction (SAED) patterns of polycrystal were observed in both Mg@HAp (Ca/Mg = 5) and Mg@HAp-PC (Ca/Mg = 5). The diffraction patterns belonging to (2 1 1) face of HAp correspond to a diffraction angle of XRD with Cu Kα source at 31.86°, which can be confirmed by the results in Fig. 2 (b) as well. It is supposed that the PC provides the confined space and inhibits the crystallization process. The crystallinity is lower in the PC system than the system in absence of PC.

The dark-field images in the same areas as the SAED are shown in Fig. 3 (a-2) and (b-2) to improve the crystalline phase's contrast. Only Mg@HAp-PC (Ca/Mg = 5) possessed an orderly arrangement of nanoscale crystals. These nanoscale crystals aligned to form the bundle-like morphology with a total length around 300 nm. Literatures have mentioned that the matrix formed by organic matters can contribute

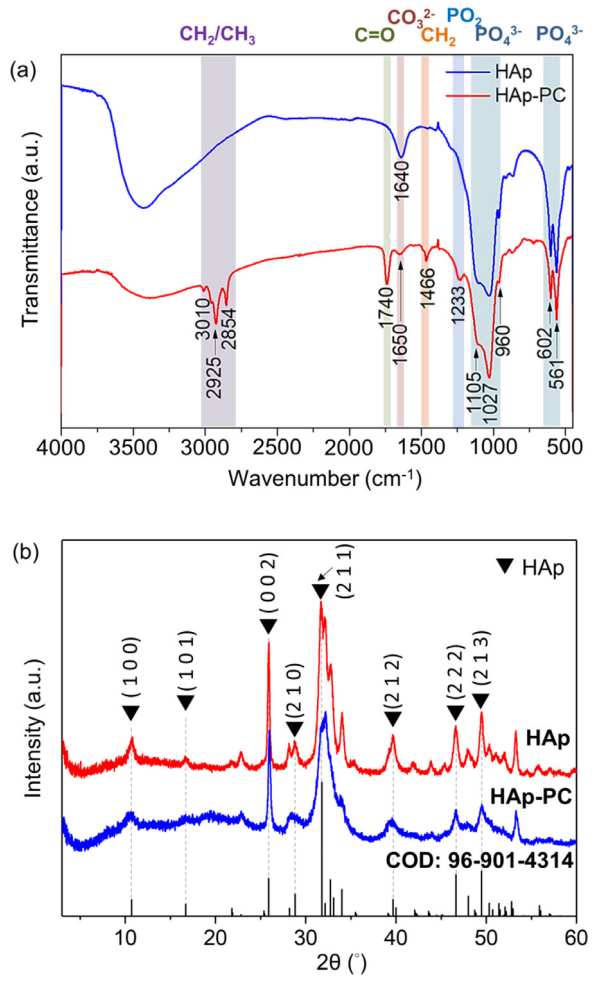

Fig. 1. (a) FTIR spectra of HAp and HAp-PC. (b) XRD Patterns of HAp and HAp-PC.

to this regular structre [53]. This arrangement is similar to the crystal arrangement of biological bone [54,55].

The effect of different Ca/Mg ratios on Mg@HAp have also been discussed. Solutions with three Ca/Mg ratios (x = 10, 5, 1) were chosen to modulate the Mg content in Mg@HAp. The XRD patterns shown in Fig. 4 reveal that the crystallinity will decreases when the portion of Mg increases. This phenomenon has been reported by literature [56]. Furthermore, comparing with the Mg@HAp-PC (Ca/Mg = 10), the corresponding peaks of Mg@HAp-PC (Ca/Mg = 5) shifted to a higher degree, owing to the increase of Mg substitution in Mg@HAp-PC.

In Fig. 5, the morphologies of Mg@HAp and Mg@HAp-PC with different Ca/Mg ratios were observed with SEM. HAp and Mg@HAp (Ca/Mg = 10) were agglomerated needle-like particles (Fig. 5 (a), (c)). After introducing the PC, HAp-PC and Mg@HAp-PC (Ca/Mg = 10) become flake-like particles (Fig. 5 (b), (d)). The morphology of Mg@HAp (Ca/Mg = 5) with and without PC are also compared in Fig. 5 (e) and (f), where larger particles will form if PC is not added during synthesis. Moreover, in the PC-incorporated system, the morphology appears to be bundle-like, suggesting the crystal axis might be aligned in the same direction to form a large ordered crystal. This result is consistent with the TEM image in Fig. 3 (b-1). Significantly, particles of HAp become columnar aggregation when the Ca/Mg ratio is 1 no matter whether the PC is involved or not (Fig. 5 (g), (h)).

The zeta potentials under neutral pH value for materials are shown in Fig. 6. Compared with Mg@HAp without adding PC, the absolute value of zeta potentials after adding PC is at least twice greater. And a greatest zeta potential value of -25.83 mV can be

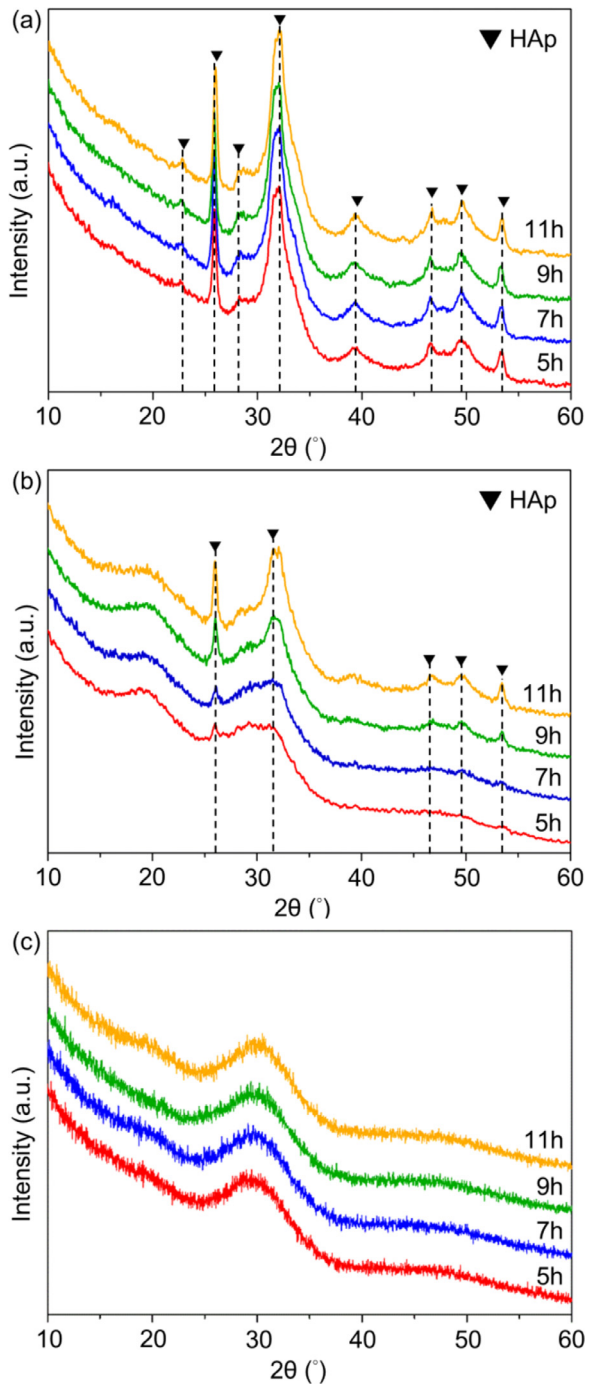

Fig. 2. The XRD patterns of (a) Mg@HAp (Ca/Mg = 5), (b) Mg@HAp-PC (Ca/Mg = 5) and (c) Mg@HAp-1.5PC (Ca/Mg = 5) after 5 to 11 h of aging.

observed from Mg@HAp-PC (Ca/Mg = 1). The negative zeta potentials of the material containing PC were attributed to the fatty acid contents in the PC we used. Literature also indicated that the negative potential of HAp can promote the deposition of calcium ions, which will participate in the formation of the extracellular matrix required for cell attachment [57,58], Because the negative zeta potential has a beneficial effect on attachment and proliferation for bone cells which has been demonstrated [59,60], we believed that our Mg@HAp-PC will be a bone material with these advantages.

To determine the amount of Ca substituted by Mg in Mg@HAp and Mg@HAp-PC, the Ca and Mg contents for each sample were analyzed by ICP-MS, and the results were shown in Table 3. The Mg content in Mg@HAp-PC can be controlled from 1.44 to 10.64 %. To better

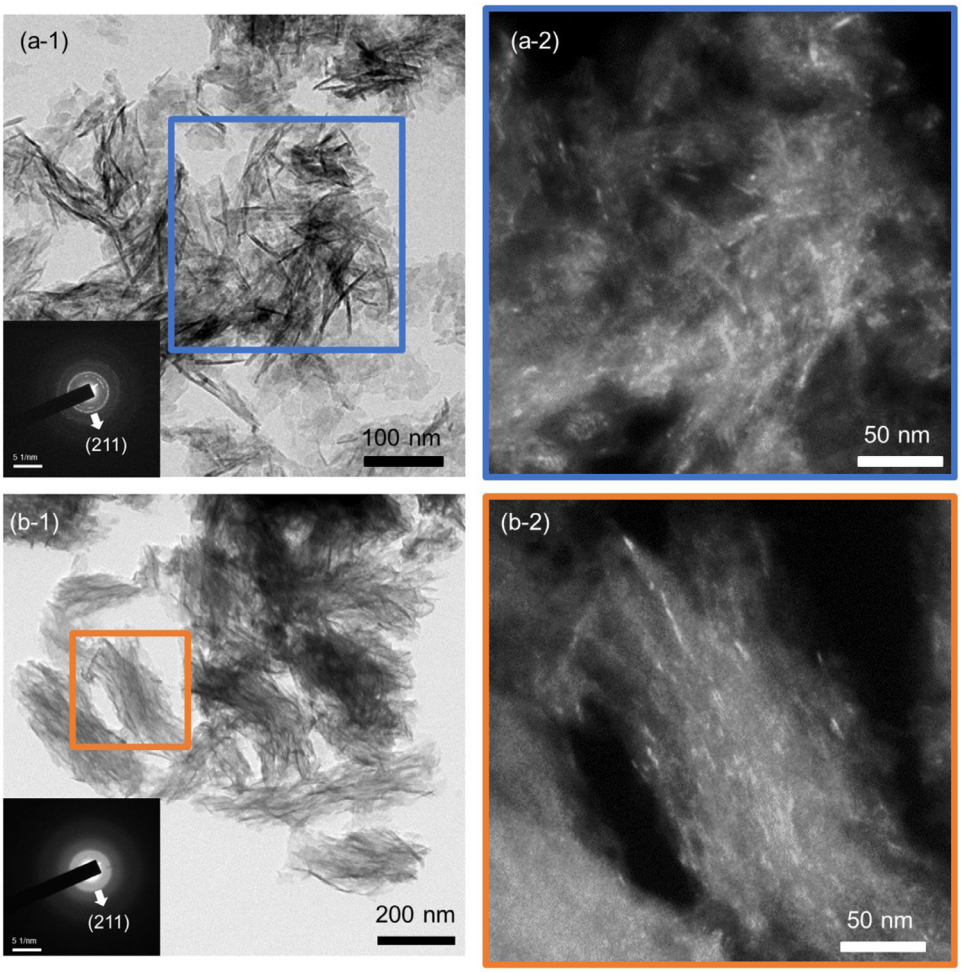

Fig. 3. The TEM images of (a) Mg@HAp (Ca/Mg = 5) and (b) Mg@HAp-PC (Ca/Mg = 5).

evaluate the composition changes in each sample, we normalized the product molar ratio and calculated the percentage of Ca replacement with the Mg and Ca/Mg ratio. Therefore, it is confirmed that PC can increase the substitution amount of Ca ions by Mg ions in Mg@HAp when the Mg concentration is high (Ca/Mg = 1). We will also design other experiments to explore the possible mechanisms of this phenomenon.

As mentioned in the introduction chapter, it is not easy to prepare a Mg@HAp with high Mg content in an aqueous system under physiological temperature. With PC's help, the Mg content of Mg@HAp can be further increased. To give a better view of how Mg is incorporated in Mg@HAp, the chemical states of magnesium and oxygen is identified with XPS (Fig. 7). The signals in the Mg2p spectra are detected on the surfaces, indicating the presence of Mg. We further use FTIR to analyze the functional groups in Mg@HAp and Mg@HAp-PC (Ca/Mg = 5) (Fig. 8). The FTIR spectra are the same as in Fig. 1 (b), where we can find the vibration modes of PO_4^{3-} and CO_3^{2-} in both samples. The difference between the spectra of Mg@HAp and Mg@HAp-PC (Ca/Mg = 5) is that the latter has an additional carbonyl band at 1740 cm^{-1} and the $\delta(CH_2)$ scissoring vibrations, which are corresponding to PC. We then use this information of functional groups to analyze the XPS spectra in Fig. 7. The chemical state of Mg@HAp and Mg@HAp-PC (Ca/Mg = 5) derived Mg-O from carbonate (red line) shows the peak belonged to Mg2p with Mg^{2+} peak around 51.9 eV [61], which is in accordance with the results obtained from the O1s spectra. Mg@HAp-PC has 6 % Mg binding with carbonate, less than 16 % that Mg@HAp has. Some studies indicated that carbonates replace the phosphate ions in the crystal structure and impact its ability to accommodate other foreign ions [62]. Therefore, this result can explain why high Mg content in Mg@HAp-PC is not entirely attributed to carbonate. It is indirectly explained that Mg content increased mainly by PC's assistance instead of carbonate for the Mg@HAp-PC.

As shown in O1s spectra, it could be observed the binding energy at 534.8 eV and 536.5 eV might be respectively assigned to PO_4^{3-} and adsorbed water [63–65]. Additionally, a peak observed at 532.2 eV in Mg@HAp (Ca/Mg = 5) is attributed to the CO_3^{2-} bond [66]. Furthermore, the binding energy of 532.1 eV and 534.4 eV may be attributed to ester C=O and O=C-O [67], respectively, and the existence of PC is also confirmed.

3.2. Proposed PC-assisted reaction mechanism

In this section, how PC can increase the Mg in Mg@HAp has been investigated. When we add the solution containing Ca and Mg ions into the round-bottom flask containing PC, the Ca and Mg in the solution will be adsorbed on the surface of the lipid membrane (Fig. 9 (a)). When we further add phosphate solution, Mg@HAp crystals will nucleate on the lipid membrane contains Ca and Mg ions, make it easier for Mg ions to be doped into HAp. We also did another experiment to prove our hypothesis (Fig. 9 (b)). In this experiment, we first added the solution containing only Ca ions to the round-bottom flask containing PC and waited for 30 min, waiting for the lipid membrane to saturate with Ca ions before adding the solution of Mg ions. In this way, we expected that Mg ions cannot easily participate the nucleation process and thus have a lower concentration in Mg@HAp. The results obtained here also indicate that for the

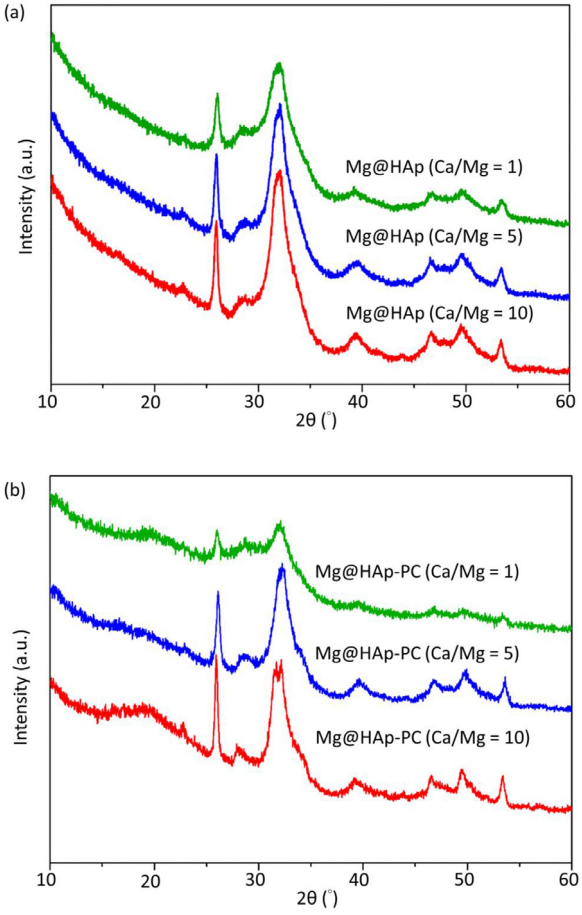

Fig. 4. The XRD patterns of (a) Mg@HAp (Ca/Mg=1, 5, 10) (b) Mg@HAp-PC (Ca/Mg = 1, 5, 10).

Table 3
The ICP-MS results of Mg@HAp and Mg@HAp-PC.

Sample	Mg (wt %)	Ca replaced by Mg Mg/(Mg+Ca)(%)	Ca/Mg (-)
Mg@HAp (Ca/Mg = 10)	1.48	8.02	11.48
Mg@HAp-PC (Ca/Mg = 10)	1.44	8.77	10.40
Mg@HAp (Ca/Mg = 5)	2.48	13.37	6.48
Mg@HAp-PC (Ca/Mg = 5)	2.58	16.08	5.22
Mg@HAp (Ca/Mg = 1)	8.36	41.98	1.38
Mg@HAp-PC (Ca/Mg = 1)	10.64	51.24	0.95

condition of Ca-occupied PC, the amount of Ca replacement with Mg indeed decreases to 14.28 %(Table 4). Which in line with our expectations.

3.3. Degradation test

The weight change for various periods was examined to determine the degradation behavior of HAp and HAp-PC powder (Fig. 10). The degradation rate of samples could be controlled from 9.43 to 28.06 % in 4 weeks of immersion in PBS. For the same ratio of Ca to Mg, the addition of PC significantly increases the degradation rate of the HAp. A higher concentration of Mg in the HAp also increases the degradation rate. The main effect of the increase in degradation rate is the Mg content in HAp, which is consistent with the early study [20,29]. Beside, the controllable degradation rate maybe match the rate of new bone formation.

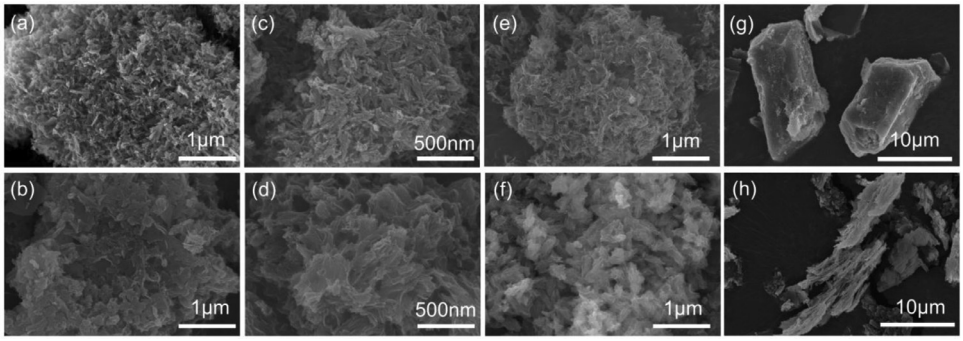

Fig. 5. SEM images of (a) HAp, (b) HAp-PC, (c) Mg@HAp (Ca/Mg = 10), (d) Mg@HAp-PC (Ca/Mg = 10), (e) Mg@HAp (Ca/Mg = 5), (f) Mg@HAp-PC (Ca/Mg = 5), (g) Mg@HAp (Ca/Mg = 1), (h) Mg@HAp-PC (Ca/Mg = 1).

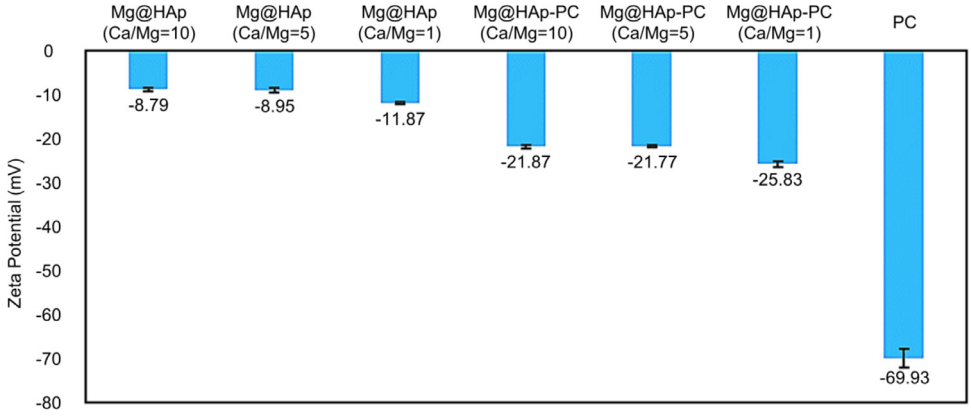

Fig. 6. Zeta potentials of Mg@HAp, Mg@HAp-PC with various of Ca/Mg ratio and PC under neutral pH value.

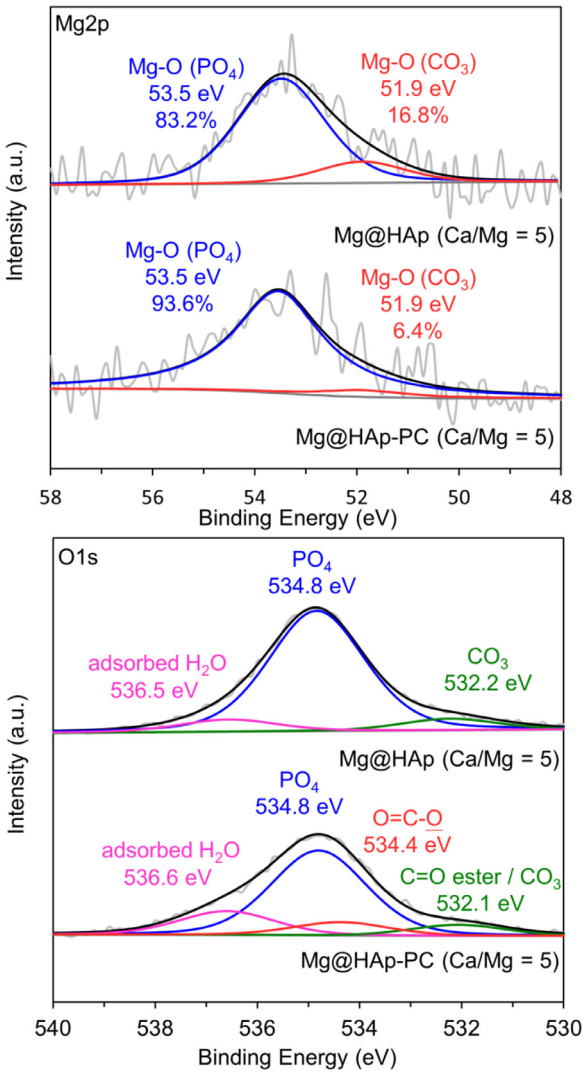

Fig. 7. XPS spectra of Mg@HAp and Mg@HAp-PC (Ca/Mg = 5).

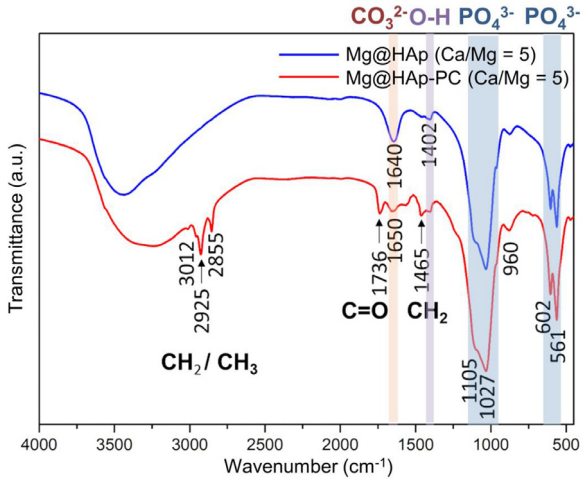

Fig. 8. FTIR analysis of Mg@HAp and Mg@HAp-PC (Ca/Mg = 5).

3.4. In vitro *test*

Various concentrations of Mg@HAp and Mg@HAp-PC were added into the culture medium of the MG-63 cell line to evaluate the biocompatibility. The MTT assay results of MG-63 cells in 1 day are shown in Fig. 11. All the materials have good biocompatibility that the cell viability is above 80% for different concentrations after 1 day of incubation. Especially for HAp-PC (Ca/Mg = 1) in 10 mg/mL, the cell viability can be as high as 221%. Although the HAp-PC (Ca/Mg = 1) in 10 mg/mL has the best effect for cell viability, the other samples are the opposite effect. Therefore, we chose 1 mg/mL as the appropriate concentration of cell proliferation tests in the 3, 5, 7, and 14 days of culture (Fig. 12). The result shows that the HAp-PC has higher cell viability compared with HAp.

Moreover, the cell viability of all materials is outstandingly different from the control group after 2 weeks. There are significant differences between HAp-PC (Ca/Mg = 5) and HAp-PC (Ca/Mg = 1) after the

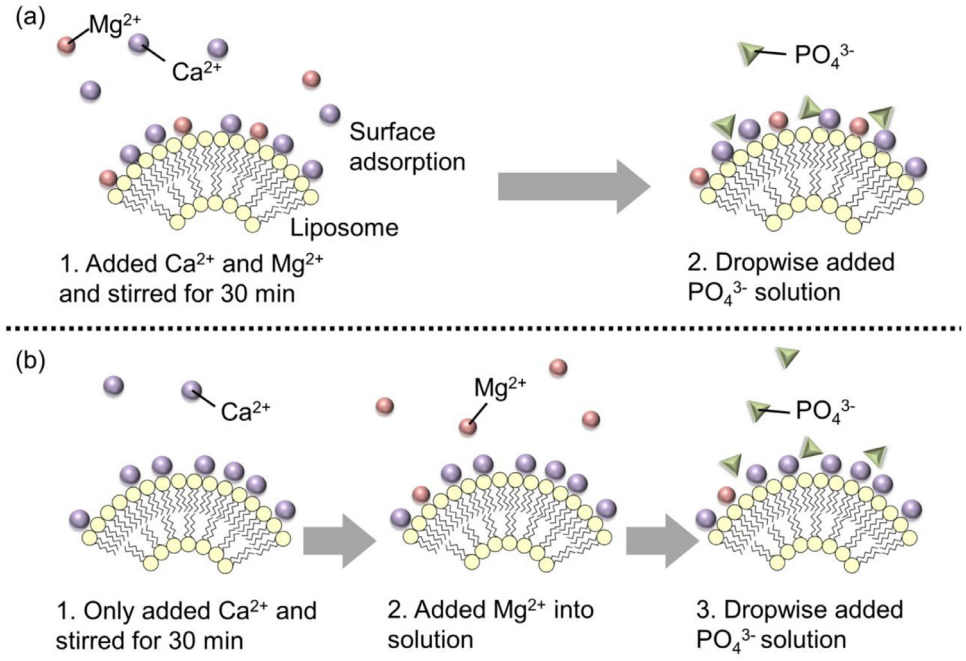

Fig. 9. (a) Nucleation of Mg@HAp (Ca/Mg = 5) on lipid membrane. (b) Modified process for preparing Mg@HAp-Ca occupied PC (Ca/Mg = 5).

Table 4
ICP-MS results of Mg@HAp-PC synthesized by different process.

Sample	ICP Ca replacement with Mg Mg/(Mg +Ca) (%)	Ca/Mg (-)
Mg@HAp-PC (Ca/Mg = 5)	16.08	5.22
Mg@HAp-Ca occupied PC (Ca/Mg = 5)	14.28	6.00

5 days of culture. It indicates that high Mg content in HAp and the addition of PC are beneficial to cellular proliferation.

ALP activity is often used to demonstrate the differentiation of bone cells. ALP activity increases when bone cells undergo the mineralization process. The ALP concentrations of HAp and Mg@HAp-PC after 3, 5, 7, and 14 days are shown in Fig. 13. It shows that the ALP concentrations of all the groups with added materials are higher than that of the control group. In particular, HAp-PC (Ca / Mg = 1) was 97% higher than the control main after 14 days. It indicated that Mg@HAp-PC can promote the differentiation of osteoblast-like cell MG-63 and help it enter the stage of mineralization.

3.5. Quantitative analysis of Mg ions release

It has been demonstrated that Mg ions can increase adhesion, growth, and ALP activity of bone cell.[19] We analyze the release concentration from the material and cellular uptake of magnesium ion after three days to investigate the causes of increased cell proliferation and differentiation. Because the best bioactivity effect of the ratio of Ca to Mg is 1, we chose this ratio to investigate. From Table 5, we can indicate the released 0.89 wt% of Mg ions for HAp-PC (Ca/Mg = 1) in 3 days, which is higher than 0.74 wt% of HAp (Ca/Mg = 1). The Mg ions uptaken by cells are 0.12 and 0.14 wt% for HAp and HAp-PC (Ca/Mg = 1). Consequently, it showed that when the Mg ions release and the concentration increased, the viability and ALP concentration increased. This phenomenon, which benefits cell proliferation and differentiation, is relative to the concentration of Mg ion release.

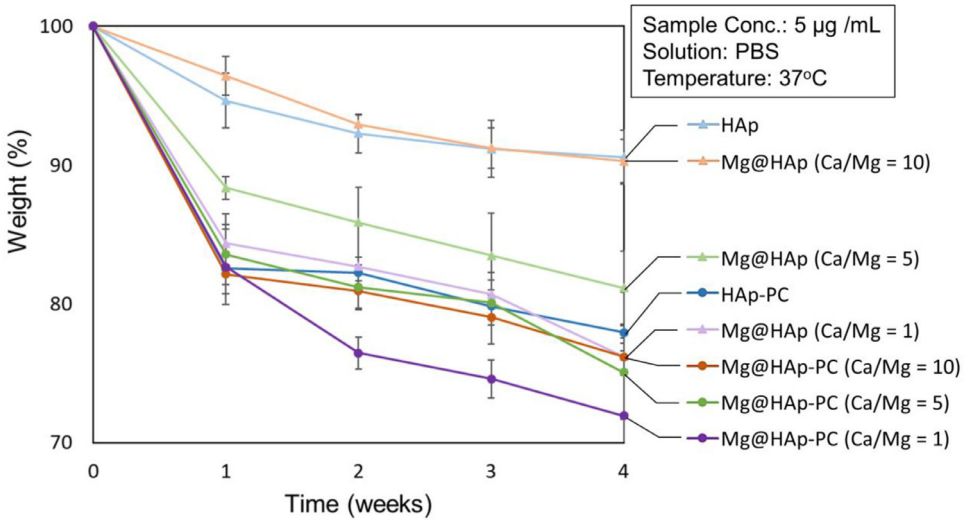

Fig. 10. Weight losses of Mg@HAp and Mg@HAp-PC after different times of degradation.

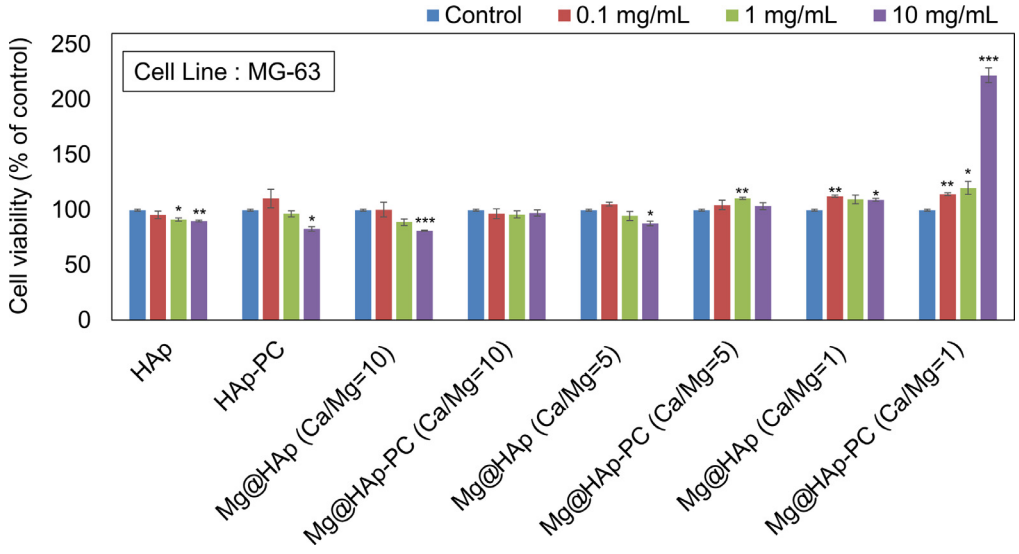

Fig. 11. Cytotoxicity of various concentrations of Mg@HAp and Mg@HAp-PC after 1 day of culture.

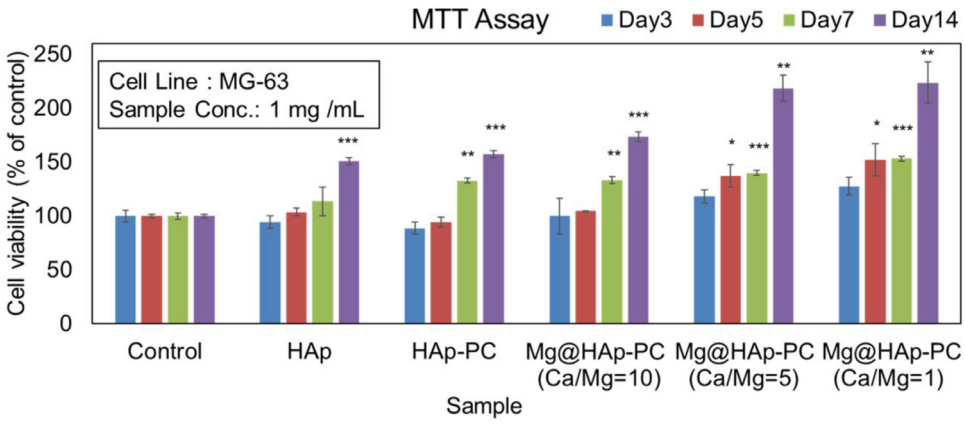

Fig. 12. Proliferation assay of MG-63 cells with HAp and Mg@HAp-PC.

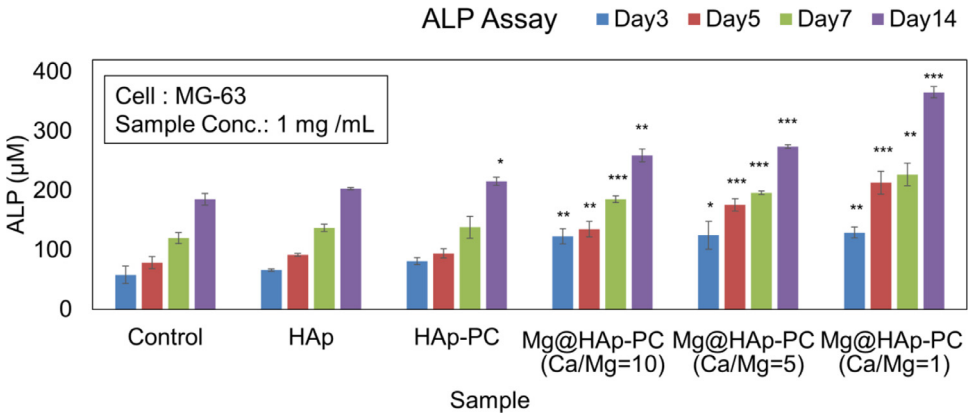

Fig. 13. ALP assay of MG-63 cells with HAp and Mg@HAp-PC.

Table 5
The Mg ions released from materials and the amount uptaken by cells in 3 days.

Sample	Mg (wt %)	Release of Mg^{2+} (wt %)	Mg^{2+} uptaked by cells (wt %)	Viability (% of control)	Viability (% of control)
Mg@HAp (Ca/Mg) = 1	8.36	0.74 ± 0.04	0.12 ± 0.05	107.92	170.75
Mg@HAp-PC (Ca/Mg) = 1	10.64	0.89 ± 0.06	0.14 ± 0.09	127.53	222.55
Data represent the mean SD for three replicates					

4. Conclusion

We had successfully synthesized Mg@HAp and Mg@HAp-PC with the Ca/Mg ratio 10, 5, and 1. The addition of the PC affects the crystallinity and the time of the crystallization of HAp. Moreover, it is indicated that the formation of the orderly crystal alignment is attributed to the PC organic matrix's presence. PC increases the loading amount of Mg and enables us to control the Mg content in Mg@HAp-PC from 1.44 to 10.64 wt%. Increasing the Mg content in HAp mainly by the assistance of PC instead of carbonate has also been confirmed. The proposed mechanism indicates that PC provides a nucleation site for Mg@HAp and helps Mg ions to enter the crystal of Mg@HAp-PC. The degradation rate for Mg@HAp could be controlled in a range from 9.71 to 28.06 % in 4 weeks. The degradation rate's primary factor is the Mg content in Mg@HAp; increasing Mg content resulted in lower crystallinity, higher degradation rate. For *in vitro* test, there is 0.89 wt% Mg ions release from HAp-PC (Ca/Mg = 1). After three days of culture, the cellular viability reached 127 % and the ALP concentration reached 222%. The presence of high Mg and the addition of PC in HAp are beneficial to cellular proliferation and differentiation, and the release of Mg ions is a significant factor for promotion. Consider all, this work reveals a novel efficacy for PC applied in Mg@HAp, providing a promising biomaterial in orthopedic applications).

Declaration of Competing Interest

The authors declare no competing financial interest.

Acknowledgment

The authors acknowledge the financial support by the Ministry of Science and Technology (MOST), Taiwan 108-2638-E-002-003-MY2 (Shackleton Program award) and National Taiwan University (NTU-AS-108L104306).

Supplementary materials

Supplementary material associated with this article can be found, in the online version, at doi:10.1016/j.jtice.2021.09.019.

References

[1] Dimitriou R, Jones E, McGonagle D, Giannoudis PV. Bone regeneration: current concepts and future directions. BMC Med 2011;9(1):66. doi: 10.1186/1741-7015-9-66.

[2] Einhorn TA. The cell and molecular biology of fracture healing. Clin Orthop Relat Res 1998(355 Suppl):S7–21. doi: 10.1097/00003086-199810001-00003.

[3] Atala A. Tissue engineering and regenerative medicine: concepts for clinical application. Rejuvenation Res 2004;7(1):15–31. doi: 10.1089/154916804323105053.

[4] Kluin OS, Van der Mei HC, Busscher HJ, Neut D. Biodegradable vs non-biodegradable antibiotic delivery devices in the treatment of osteomyelitis. Expert Opin. Drug Deliv 2013;10(3):341–51.

[5] Arora M, Chan EK, Gupta S, Diwan AD. Polymethylmethacrylate bone cements and additives: a review of the literature. World J. Orthop. 2013;4(2):67.

[6] Berzina-Cimdina L, Borodajenko N. Research of calcium phosphates using Fourier transform infrared spectroscopy. Infrared Spectrosc. Mater. Sci. Eng. Technol. 2012;12(7):251–63.

[7] Hannink G, Arts JJ. Bioresorbability, porosity and mechanical strength of bone substitutes: what is optimal for bone regeneration? Injury 2011;42(Suppl 2): S22–5. doi: 10.1016/j.injury.2011.06.008.

[8] Hench LL, Polak JM. Third-generation biomedical materials. Science 2002;295 (5557):1014–7.

[9] Shuai C, Yu L, Yang W, Peng S, Zhong Y, Feng P. Phosphonic acid coupling agent modification of HAP nanoparticles: interfacial effects in PLLA/HAP bone scaffold. Polymers 2020;12(1):199.

[10] Kaseem M, Choe HC. Triggering the hydroxyapatite deposition on the surface of PEO-coated Ti−6Al−4V alloy via the dual incorporation of Zn and Mg ions. J Alloy Compd 2020;819:153038. doi: 10.1016/j.jallcom.2019.153038.

[11] Yokoi T, Goto T, Kato T, Takahashi S, Nakamura J, Sekino T, Ohtsuki C, Kawashita M. Hydroxyapatite formation from octacalcium phosphate and its related compounds: a discussion of the transformation mechanism. Bull Chem Soc Jpn 2020;93(5):701–7. doi: 10.1246/bcsj.20200031.

[12] Yang X, Wang Z. Synthesis of biphasic ceramics of hydroxyapatite and β-tricalcium phosphate with controlled phase content and porosity. J Mater Chem 1998;8(10):2233–7. doi: 10.1039/A802067A.

[13] Gallinetti S, Canal C, Ginebra MP. Development and characterization of biphasic hydroxyapatite/β-TCP cements. J Am Ceram Soc 2014;97(4):1065–73. doi: 10.1111/jace.12861.

[14] Sadat-Shojai M, Khorasani MT, Dinpanah-Khoshdargi E, Jamshidi A. Synthesis methods for nanosized hydroxyapatite with diverse structures. Acta Biomater 2013;9(8):7591–621. doi: 10.1016/j.actbio.2013.04.012.

[15] Stevens MM. Biomaterials for bone tissue engineering. Mater Today 2008;11 (5):18–25. doi: 10.1016/S1369-7021(08)70086-5.

[16] Burg KJ, Porter S, Kellam JF. Biomaterial developments for bone tissue engineering. Biomaterials 2000;21(23):2347–59. doi: 10.1016/s0142-9612(00)00102-2.

[17] Rezwan K, Chen QZ, Blaker JJ, Boccaccini AR. Biodegradable and bioactive porous polymer/inorganic composite scaffolds for bone tissue engineering. Biomaterials 2006;27(18):3413–31. doi: 10.1016/j.biomaterials.2006.01.039.

[18] Rey C, Combes C, Drouet C, Glimcher MJ. Bone mineral: update on chemical composition and structure. Osteoporosis Int 2009;20(6):1013–21.

[19] Gozalian A, Behnamghader A, Daliri M, Moshkforoush A. Synthesis and thermal behavior of Mg-doped calcium phosphate nanopowders via the sol gel method. Sci Iran 2011;18(6):1614–22. doi: 10.1016/j.scient.2011.11.014.

[20] Zilm ME, Chen L, Sharma V, McDannald A, Jain M, Ramprasad R, Wei M. Hydroxyapatite substituted by transition metals: experiment and theory. Phys Chem Chem Phys 2016;18(24):16457–65. doi: 10.1039/C6CP00474A.

[21] Landi E, Logroscino G, Proietti L, Tampieri A, Sandri M, Sprio S. Biomimetic Mg-substituted hydroxyapatite: from synthesis to *in vivo* behavior. J Mater Sci Mater Med 2008;19(1):239–47. doi: 10.1007/s10856-006-0032-y.

[22] LeGeros RZ. Calcium phosphates in oral biology and medicine. Monogr Oral Sci 1991;15:1–201.

[23] Jahnen-Dechent W, Ketteler M. Magnesium basics. Clin Kidney J 2012;5(Suppl_1): i3–i14. doi: 10.1093/ndtplus/sfr163.

[24] Liangzhi G, Weibin Z, Yuhui S. Magnesium substituted hydroxyapatite whiskers: synthesis, characterization and bioactivity evaluation. RSC Adv 2016;6 (115):114707–13. doi: 10.1039/C6RA24469F.

[25] Zhang Y, Xu J, Ruan YC, Yu MK, O'Laughlin M, Wise H, Chen D, Tian L, Shi D, Wang J, Chen S, Feng JQ, Chow DHK, Xie X, Zheng L, Huang L, Huang S, Leung K, Lu N, Zhao L, Li H, Zhao D, Guo X, Chan K, Witte F, Chan HC, Zheng Y, Qin L. Implant-derived magnesium induces local neuronal production of CGRP to improve bone-fracture healing in rats. Nat Med 2016;22(10):1160–9. doi: 10.1038/nm.4162.

[26] Chaudhry AA, Goodall J, Vickers M, Cockcroft JK, Rehman I, Knowles JC, Darr JA. Synthesis and characterization of magnesium substituted calcium phosphate bioceramic nanoparticles made via continuous hydrothermal flow synthesis. J Mater Chem 2008;18(48):5900–8. doi: 10.1039/B807920J.

[27] Lenders JJM, Dey A, Bomans PHH, Spielmann J, Hendrix MMRM, de With G, Meldrum FC, Harder S, Sommerdijk NAJM. High-magnesian calcite mesocrystals: a coordination chemistry approach. J Am Chem Soc 2012;134(2):1367–73. doi: 10.1021/ja210791p.

[28] Bertoni E, Bigi A, Cojazzi G, Gandolfi M, Panzavolta S, Roveri N. Nanocrystals of magnesium and fluoride substituted hydroxyapatite. J Inorg Biochem 1998;72(1-2):29–35. doi: 10.1016/s0162-0134(98)10058-2.

[29] Xu J, Yan C, Zhang F, Konishi H, Xu H, Teng HH. Testing the cation-hydration effect on the crystallization of Ca−Mg−CO_3systems. Proc Natl Acad Sci 2013;110 (44):17750–5. doi: 10.1073/pnas.1307612110.

[30] Ren F, Leng Y, Xin R, Ge X. Synthesis, characterization and ab initio simulation of magnesium-substituted hydroxyapatite. Acta Biomater 2010;6(7):2787–96. doi: 10.1016/j.actbio.2009.12.044.

[31] Cacciotti I, Bianco A, Lombardi M, Montanaro L. Mg-substituted hydroxyapatite nanopowders: synthesis, thermal stability and sintering behavior. J Eur Ceram Soc 2009;29(14):2969–78. doi: 10.1016/j.jeurceramsoc.2009.04.038.

[32] Suchanek WL, Byrappa K, Shuk P, Riman RE, Janas VF, TenHuisen KS. Preparation of magnesium-substituted hydroxyapatite powders by the mechanochemical-hydrothermal method. Biomaterials 2004;25(19):4647–57. doi: 10.1016/j.biomaterials.2003.12.008.

[33] Laurencin D, Almora-Barrios N, de Leeuw NH, Gervais C, Bonhomme C, Mauri F, Chrzanowski W, Knowles JC, Newport RJ, Wong A, Gan Z, Smith ME. Magnesium incorporation into hydroxyapatite. Biomaterials 2011;32(7):1826–37. doi: 10.1016/j.biomaterials.2010.11.017.

[34] Feng Q, Chen Q, Wang H, Cui F. Influence of concentration of calcium ion on controlled precipitation of calcium phosphate within unilamellar lipid vesicles. J Cryst Growth 1998;186(1-2):245–50.

[35] Chu M, Liu G. Preparation and characterization of hydroxyapatite/liposome core−shell nanocomposites. Nanotechnology 2005;16(8):1208.

[36] Huang JS, Liu KM, Chen CC, Ho KY, Wu YM, Wang CC, Cheng YM, Ko WL, Liu CS, Ho YP, Wang YP, Hong K. Liposomes-coated hydroxyapatite and tricalcium phosphate implanted in the mandibular bony defect of miniature swine. Kaohsiung J Med Sci 1997;13(4):213–28.

[37] Esko JD, Raetz C. Autoradiographic detection of animal cell membrane mutants altered in phosphatidylcholine synthesis. Proc Natl Acad Sci 1980;77(9):5192–6.

[38] Phillips R, Ursell T, Wiggins P, Sens P. Emerging roles for lipids in shaping membrane-protein function. Nature 2009;459(7245):379–85. doi: 10.1038/nature08147.

[39] Perttu EK, Szoka FC. Zwitterionic sulfobetaine lipids that form vesicles with salt-dependent thermotropic properties. Chem Commun 2011;47(47):12613–5. doi: 10.1039/C1CC15804J.

[40] Szcześ A. Effects of DPPC/cholesterol liposomes on the properties of freshly precipitated calcium carbonate. Colloids Surf B Biointerfaces 2013;101:44–8.

[41] Lis L, Lis W, Parsegian V, Rand R. Adsorption of divalent cations to a variety of phosphatidylcholine bilayers. Biochemistry 1981;20(7):1771–7.

[42] Yu PT, Tsao C, Wang CC, Chang CY, Wang CH, Chan JCC. High-magnesium calcite mesocrystals: formation in aqueous solution under ambient conditions. Angew Chem 2017;129(51):16420–4.

[43] Kuete V, Karaosmanoğlu O, Sivas H. Anticancer Activities of African medicinal spices and vegetables. In: Kuete V, editor. Medicinal spices and vegetables from Africa. Cambridge, Massachusetts: Academic Press; 2017. p. 271–97.

[44] Sanikop S, Patil S, Agrawal P. Gingival crevicular fluid alkaline phosphatase as a potential diagnostic marker of periodontal disease. J Indian Soc Periodontol 2012;16(4):513.

[45] Brundavanam S, Poinern GEJ, Fawcett D. Kinetic and adsorption behavior of aqueous Fe2+, Cu2+ and Zn2+ using a 30 nm hydroxyapatite based powder synthesized via a combined ultrasound and microwave based technique. Am J Mater Sci 2015;5(2):31–40.

[46] Nassif N, Martineau F, Syzgantseva O, Gobeaux F, Willinger M, Coradin T, Cassaignon S, Azaïs T, Giraud-Guille MM. *In vivo* inspired conditions to synthesize biomimetic hydroxyapatite. Chem Mater 2010;22(12):3653–63.

[47] Ren F, Ding Y, Leng Y. Infrared spectroscopic characterization of carbonated apatite: a combined experimental and computational study. J Biomed Mater Res Part A 2014;102(2):496–505.

[48] Destainville A, Champion E, Bernache-Assollant D, Laborde E. Synthesis, characterization and thermal behavior of apatitic tricalcium phosphate. Mater Chem Phys 2003;80(1):269–77.

[49] Raynaud S, Champion E, Bernache-Assollant D, Thomas P. Calcium phosphate apatites with variable Ca/P atomic ratio I. Synthesis, characterization and thermal stability of powders. Biomaterials 2002;23(4):1065–72.

[50] Meejoo S, Maneeprakorn W, Winotai P. Phase and thermal stability of nanocrystalline hydroxyapatite prepared via microwave heating. Thermochim Acta 2006;447(1):115–20.

[51] Bridelli MG, Capelletti R, Mora C. Structural features and functional properties of water in model DMPC membranes: thermally stimulated depolarization currents (TSDCs) and Fourier transform infrared (FTIR) studies. J Phys D Appl Phys 2013;46(48):485401. doi: 10.1088/0022-3727/46/48/485401.

[52] Cagnasso M, Boero V, Franchini MA, Chorover J. ATR-FTIR studies of phospholipid vesicle interactions with α-FeOOH and α-Fe_2O_3 surfaces. Colloids Surf. B. Biointerfaces 2010;76(2):456–67.

[53] Sturm EV, Cölfen H. Mesocrystals: structural and morphogenetic aspects. Chem Soc Rev 2016;45(21):5821–33.

[54] Schwarcz HP, McNally EA, Botton GA. Dark-field transmission electron microscopy of cortical bone reveals details of extrafibrillar crystals. J Struct Biol 2014;188(3):240–8.

[55] Ziv V, Wagner H, Weiner S. Microstructure-microhardness relations in parallel-fibered and lamellar bone. Bone 1996;18(5):417–28.

[56] LeGeros RZ. Calcium phosphate-based osteoinductive materials. Chem Rev 2008;108(11):4742–53.

[57] Cheng K, Weng W, Wang H, Zhang S. *In vitro* behavior of osteoblast-like cells on fluoridated hydroxyapatite coatings. Biomaterials 2005;26(32):6288–95.

[58] Fahami A, Beall GW, Betancourt T. Synthesis, bioactivity and zeta potential investigations of chlorine and fluorine substituted hydroxyapatite. Mater Sci Eng C 2016;59:78–85.

[59] Smeets R, Kolk A, Gerressen M, Driemel O, Maciejewski O, Hermanns-Sachweh B, Riediger D, Stein JM. A new biphasic osteoinductive calcium composite material

with a negative Zeta potential for bone augmentation. Head Face Med 2009;5(1):1–8.
[60] Fahami A, Beall GW. Mechanosynthesis of carbonate doped chlorapatite–ZnO nanocomposite with negative zeta potential. Ceram Int 2015;41(9):12323–30.
[61] Fournier V, Marcus P, Olefjord I. Oxidation of magnesium. Surf Interface Anal 2002;34(1):494–7.
[62] Mayer I, Schlam R, Featherstone J. Magnesium-containing carbonate apatites. J Inorg Biochem 1997;66(1):1–6.
[63] Wang J, Chao Y, Wan Q, Zhu Z, Yu H. Fluoridated hydroxyapatite coatings on titanium obtained by electrochemical deposition. Acta Biomater 2009;5(5):1798–807.
[64] Chen K, Xie K, Long Q, Deng L, Fu Z, Xiao H, Xie L. Fabrication of core–shell Ag@pDA@ HAp nanoparticles with the ability for controlled release of Ag+ and superior hemocompatibility. RSC Adv 2017;7(47):29368–77.
[65] Kačiulis S, Mattogno G, Pandolfi L, Cavalli M, Gnappi G, Montenero A. XPS study of apatite-based coatings prepared by sol–gel technique. Appl Surf Sci 1999;151(1-2):1–5.
[66] Khairallah F, Glisenti A. XPS study of MgO nanopowders obtained by different preparation procedures. Surf Sci Spectra 2006;13(1):58–71.
[67] Sivaranjini B, Mangaiyarkarasi R, Ganesh V, Umadevi S. Vertical alignment of liquid crystals over a functionalized flexible substrate. Sci Rep 2018;8(1):1–13.